INVESTIGATIONS OF NEAR-WALL BUBBLE BEHAVIOR IN WIRE HEATERS POOL BOILING

by

Kailun GUO [a,b]**,** ***Chenglong WANG*** [a,b]**,** ***Dalin ZHANG*** [a,b]**,** ***Wenxi TIAN*** [a,b]**,**
Guanghui SU [a,b]**, and** ***Suizheng QIU*** [a,b*]

[a] School of Nuclear Science and Technology, Xi'an Jiaotong University, Xi'an, China
[b] State Key Laboratory of Multi-phase Flow in Power Engineering, Xi'an Jiaotong University, Xi'an, China

Original scientific paper
https://doi.org/10.2298/TSCI200408333G

Current work establishes a pool boiling critical heat flux prediction method based on percolation theory. For the first time, we observe the experimental bubble footprint's power-law distributions with almost the same exponent in wire heaters' water pool boiling crisis, which is borne out strongly that boiling crisis is a typical continuum percolative scale-free behavior, and its characteristics seems not to be influenced by the critical heat flux value. The proposed 1-D Monte-Carlo method successfully simulates the phase transition of interactive near-wall bubbles. This research enriches and extends applications of continuum percolation theory in boiling phenomena, and could be an instruction for the followed critical heat flux enhancement studies.

Key words: *1-D continuum percolation theory, boiling crisis, critical heat flux, critical phenomena, scale-free behavior, numerical simulation, pool boiling*

Introduction

Heat transfer is essential to the economics and efficiency in a heat transmission system, *e.g.*, in chemical industry, power energy system and aerospace field. In all kind of heat transfer mechanisms, boiling heat transfer presents its unique advantages due to the high heat transfer coefficients (HTC) during the process. Such a high HTC near the heated surface is mainly caused by the heat transport due to the phase change and strong disturbances between vapor and liquid in nucleate boiling regime. Generally, the higher heat flux/wall super heat is, the more bubble nucleation sites and higher bubble departure frequency will be, resulting in a higher HTC. However, the limit of the nucleate boiling heat transfer, the so-called critical heat flux (CHF), will dramatically deteriorate the heat transfer efficiency by quickly converting the nucleate boiling regime into film boiling where a large vapor layer prevents liquid rewetting the heated surface [1]. The decrease of HTC will overheat and eventually break the boiling surface which is not acceptable in a heat transmission system. Thus, the study of the CHF enhancement and understanding the boiling mechanism are emphases to avoid the boiling crises.

From numerous experimental investigations [2-5], one can conclude that CHF is a fairly complex process which combines the influence of fluid properties, operating conditions, surface material, orientation and properties. Researchers are still trying to predict and under-

* Corresponding author, e-mail: szqiu@mail.xjtu.edu.cn

stand this puzzling phenomenon. Variety of models are developed based on presumed trigger mechanisms, including hydrodynamic instabilities [6, 7], surface wettability [8-11] and liquid microlayers [12, 13]. Although reasonable results can be achieved from those models, the consensus explanation of the vapor film formation is still not reached [14].

In past few years, the criticality of CHF is observed from a different respect. The critical phenomenon at boiling crisis is firstly reported by Skokov *et al.* [15] by observing the current signal fluctuations with a 1/f spectrum on a vertical platinum wire heater. In 2010, the acoustic emission energy distribution of heating surface in liquid nitrogen [16] and dry spot distribution in a slowed-down boiling of hydrogen at zero gravity [17] are also observed as critical phenomenon at boiling crisis. More recently, Zhang *et al.* [18] demonstrate the scale-free phenomenon into bubble footprint distributions both in pool boiling and flow boiling of water. Besides experimental observations, theoretical models proposed in [16, 18] also prove that the boiling crisis can be explained as a result of bubble percolative process [19]. The percolative scale-free characteristic of boiling crisis provides us a criterion predict CHF and open a gate to better understand the vapor film formation and near-wall bubble interactions. However, the study of scale-free phenomenon at boiling crisis is in the early stage, lots of investigations are still needed to support and enrich this theory to became widely recognized.

In this paper, we carry out the first experimental study of bubble footprint distributions along a thin wire in pool boiling of water. The wire heater boiling is chosen owe to its maneuverability and lower cost. Based on high resolution high speed videos (HSV), the bubble footprint distribution under boiling crisis is investigated. The 1-D Monte-Carlo (MC) model is proposed based on continuum percolation theory to further simulated the near-wall bubble interactions. Both experimental and simulated results show that the near-wall bubble behaviors can be explained as typical percolative process.

Theoretical analysis for 1-D continuum percolation problem

The basic idea of the 1-D site percolation is introduced in this section. First, let us imagine a chain of 1-D lattice with infinity length. If we occupy each lattice randomly with probability, p, we will get a chain as shown in fig. 1.

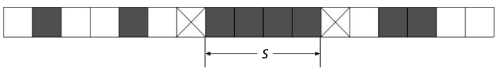

Figure 1. The 1-D site percolation problem (occupied sites are marked by gray square)

If the system scale is large enough ($L \to \infty$), we can get a cluster with size s when s sites are occupied as well as two empty sites appear on each end marked by crosses in fig. 1. The probability of the site to be the left-most site of s-cluster is [20]:

$$n(s,p) = (1-p)^2\, p^s \tag{1}$$

the $n(s, p)$ is also defined as the cluster number density.

The probability of a site belongs to a s-cluster is [20]:

$$\omega(s,p) = C_s^1 n(s,p) = s(1-p)^2\, p^s \tag{2}$$

According to eq. (2), we can get:

$$\sum_{s=1}^{\infty}\omega(s,p) = \sum_{s=1}^{\infty} s(1-p)^2\, p^s = (1-p)^2 \sum_{s=1}^{\infty} p\frac{\mathrm{d}p^s}{\mathrm{d}p} = p \tag{3}$$

Thus the probability that the occupied cluster contains s sites, *i.e.* probability density function (PDF) is:

$$f(s,p)=\frac{\omega(s,p)}{\sum_{s=1}^{\infty}\omega(s,p)}=\frac{(1-p)^2}{p}s\mathrm{e}^{\ln p\cdot s} \tag{4}$$

Then the average cluster size can be calculated:

$$S(p)=\sum_{s=1}^{\infty}sf(s,p)=\sum_{s=1}^{\infty}\frac{(1-p)^2}{p}s^2\mathrm{e}^{\ln p\cdot s}=\frac{1+p}{1-p} \tag{5}$$

Then two order parameters are defined to investigate the 1-D percolation problem:

$$P(p,L)=\frac{\mathrm{S_L}}{L},\quad P'(p,L)=\frac{s_{\mathrm{SL}}}{L} \tag{6}$$

where S_L is the longest cluster size and S_SL – the second longest cluster size in the system. So the P and P' means the density of the longest cluster and second longest cluster, respectively. According to the percolation theory, the symbol of percolation happens is the rapid growth of P and P' reaches its maximum value, this is called the phase transition phenomenon in the system.

In our research, a 1-D continuum percolation problem is proposed based on fig. 1, the 1-D chain is occupied by stripes with 2r in length instead of single sits.

Figure 2 shows simulation results of a 1-D continuum percolation system (r = 4, L = 1000), different clusters are marked by different gray scale. As shown in the figure, before the critical occupied probability, the longest and second longest cluster have almost same length, and both clusters size increase as occupied probability increases. When p = 0.6, we can clear observe that the longest cluster increases (the gray one) and the second longest cluster decreases (the black one), which means the critical phenomena occur between p = 0.5 and p = 0.6.

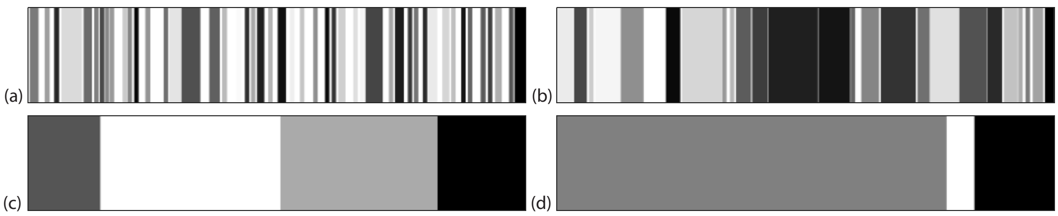

Figure 2. Simulation results for 1-D continuum percolation system (r = 4, L = 1000) under different occupied probabilities; (a) p = 0.1, (b) p = 0.3, (c) p = 0.5, and (d) p = 0.6

Figures 3 and 4 show the change of P and P' under different r and L. As shown in figures, the rapid increase of P and maximum value of P' are clearly observed in different cases. The occupied probability when the second cluster become its maximum value can be defined as the critical occupied probability. After the critical p, the density of second longest cluster rapidly decreases and finally become zero.

The critical phenomena observed in 1-D continuum percolation system are the theoretical basis of this work. The near-wall bubble behaviors in wire heaters' pool boiling test will be simulated base on the 1-D continuum percolation theory in followed sections.

Methodology of experiment and simulation

Pool boiling test facility

The pool boiling experiment apparatus is shown in fig. 5. Test section mainly consists of a glass vessel as the water bath container, two teflon covered copper rods fixed in container

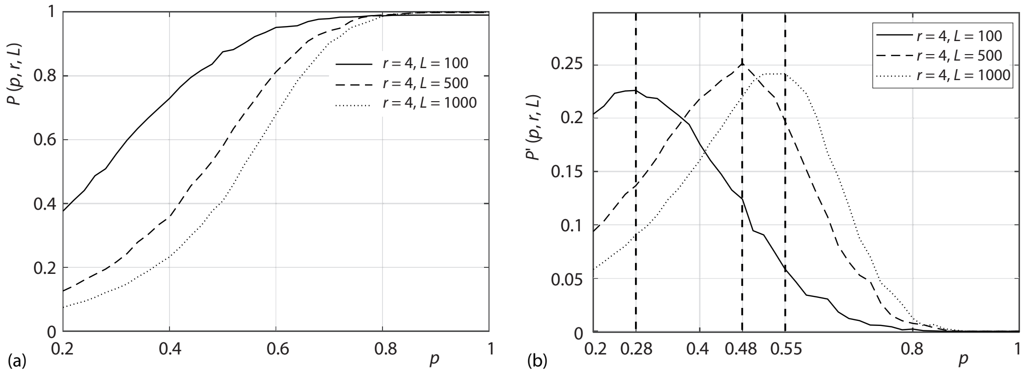

Figure 3. Density of clusters varies with occupied probability in 1-D continuum percolation system with different scales; (a) longest cluster density and (b) second longest cluster density

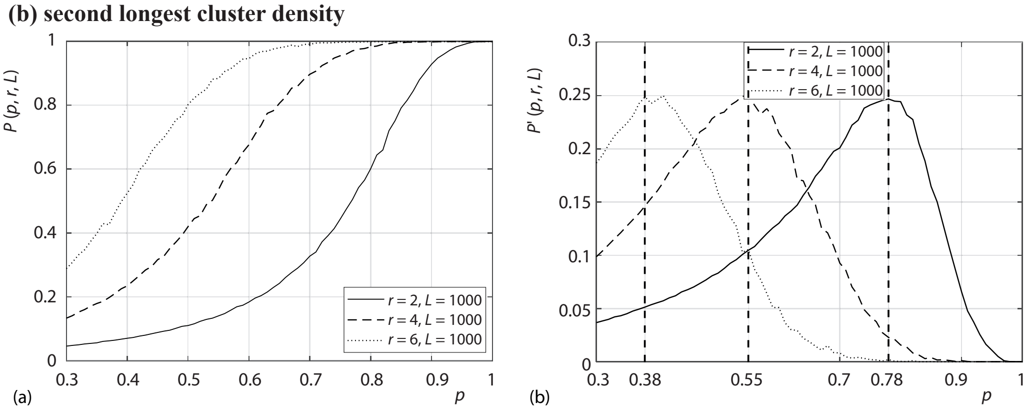

Figure 4. Density of clusters varies with occupied probability in 1-D continuum percolation system with different stripe length; (a) longest cluster density and (b) second longest cluster density

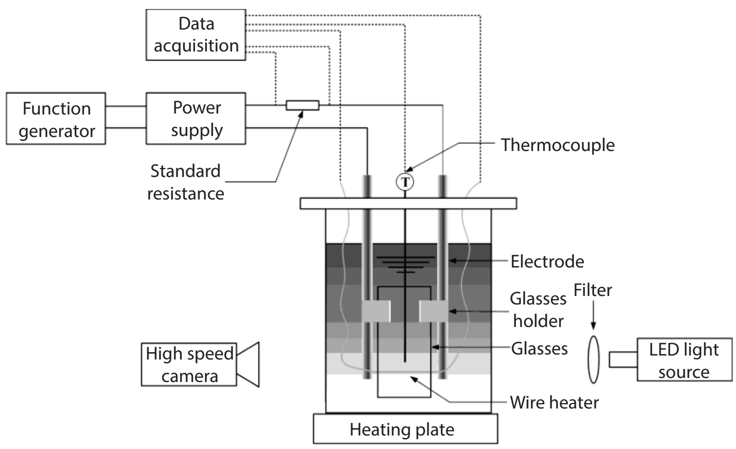

Figure 5. Schematic of the wire heater pool boiling test facility

cover are used as electrodes on which a 69.0 ±0.2 mm wire heater is soldered. A small hole in the cover maintains the atmospheric pressure in the chamber. The working fluid is preheated by the heating plate to be saturated, a *T*-type thermocouple is inserted into water to monitor the temperature.

The power is provided by the Chroma model 62050P programmable DC power supply (100 V/100 A), the power increasing is controlled by the RIGOL DG1022U function generator. When the power is close to the expected critical value, it increases in smaller steps. The agilent technologies 34980 A data acquisition system is employed to record the voltage differences over the standard resistance (Rs) (50 mV/15 A) and wire heater, as well as the fluid temperature. The whole boiling process is captured by Phantom V2512 high speed camera with Nikon ED AF MICRO NIKKOR 200 mm lens. The high speed camera control software is Phantom PCC 3.1. The frame rate for each test is 5000 fps to make sure we record adequate details of near-wall bubbles.

Image post-processing

Figure 6 shows typical frames (resolution 1024 × 256) of nucleate boiling on the different wire heaters, confined wire heaters have obvious larger bubbles due to glasses squeezing. For the sandwiched wire heaters, we only focus on the part confined by glasses (40.4 ±0.2 mm).

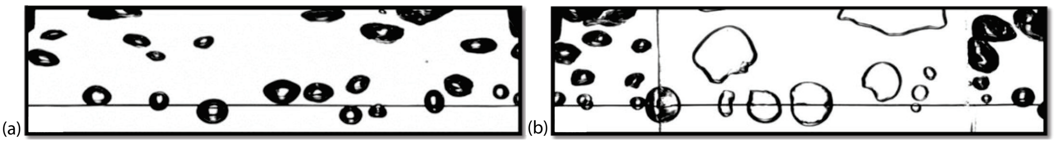

Figure 6. Typical frames of nucleate boiling on different wire heaters; (a) bare wire heater at 399 kW/m^2 and (b) sandwiched bare wire heater at 401 kW/m^2

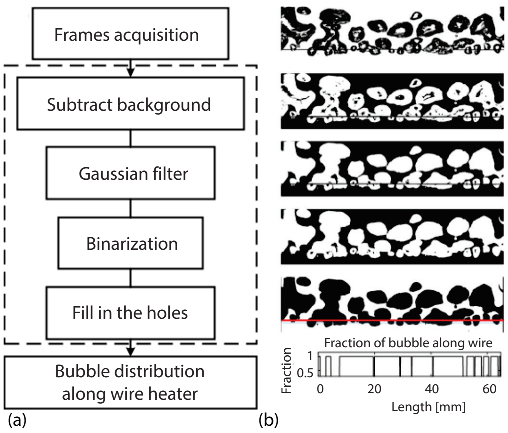

Figure 7. Image post-processing of getting the bubble size distribution along the wire heater; (a) flowchart of the methodology and (b) an application of the post-processing code on one of frames of bare wire heater's CHF (929 kW/m^2)

The bubble size along the wire heater cannot be directly obtained from high contract frames. We develop an image post-processing algorithm as shown in fig. 7(a) based on MATLAB R2018b to handle HSV frame by frame. First, we have to omit the wire heater from the frame because it is so thin that its thickness would not be uniform after binarization, resulting in difficulties in detecting the bubble footprint. So we subtract the background, which is a frame before the boiling starts, from the original frame to eliminate the influence of the wire heater. Then we apply the Gaussian filter and binarization the frame to close opened bubbles caused by the subtraction. In the filter step, we need stronger blurred effects in the *Y*-direction (normal to the wire heater) to cover the subtracted wire heater, but weaker blurred effects in the *X*-direction (along the wire heater) to make sure the bubble size won't be enlarged by the filter. Comparing with averaging filter and circular averaging filter, Gaussian filter is chosen because it allows us to specify the size of the filter element in *X*- and

Y-direction, respectively. After filling in the holes of the frame, we take a narrow stripe, marked in red in fig. 7(b), which is precisely the same position as the omitted wire heater. Finally, the bubble size distribution is indicated by the fraction of bubble along the wire heater. It is noted that all the non-zero fractions are set to be one to intuitively reflect the length of bubbles.

The Monte-Carlo model

In this paper, we proposed a MC model based on 1-D continuum percolation theory to simulate the near-wall bubble behaviors. Threes inputs are needed in the MC model: nucleation site density (NSD), growth time times bubble departure frequency, $t_g f$, and bubble size l. Here, the NSD, $t_g f$, and l are corresponding to number of sites, occupied probability and stripe length in 1-D continuum percolation system as discussed in Section *Theoretical analysis for 1-D continuum percolation problem*.

The simulation process can be summarized:

- randomly generate N nucleation sites along wire heaters,
- for each nucleation site, pick a random number $b \in [0, 1]$. If $b \leq t_g f$, generate a bubble with length l, and
- if the nucleation site is already occupied by the bubble generated from another site, skip the current loop.

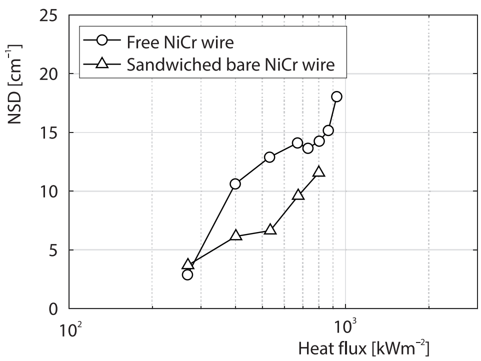

Figure 8. The NSD as a function of average heat flux

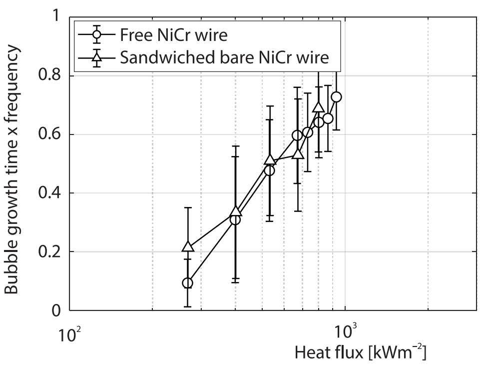

Figure 9. Product of growth time and bubble departure frequency as a function of average heat flux

Nucleation site density

The NSD is acquired from HSV. As shown in fig. 8, the sandwiched wire heater has fewer nucleation sites due to an efficient convection heat transfer improvement in confined boiling [21]. In addition, the sandwiched wire heater is easier to be occupied by bubbles due to glasses squeezing, which also reduces the possibility of nucleation sites occurrence along the wire heater.

Product of growth time and bubble departure frequency

Once we get the nucleation sites along the wire, the bubble growth time t_g and bubble wait time t_w are easy to be obtained. The bubble departure frequency f and the bubble growth time multiplies bubble departure frequency, $t_g f$, can be calculated as eqs. (7) and (8), respectively. Figure 9 shows $t_g f$ variations in each case as a function of average heat flux:

$$f = \frac{1}{t_g + t_w} \tag{7}$$

$$t_g f = \frac{t_g}{t_g + t_w} \tag{8}$$

Average bubble length

Average bubble length in the MC model refers to the length of isolated bubbles along wire heaters at different average heat flux. When the heat flux is too high, the fully developed isolated bubble can be hardly observed. So in this study, we acquire the trend of average bubble length changing from three relative low average heat flux stages with enough fully developed isolated bubbles.

In our research, we found the average bubble length PDF distribution follows the trends of cluster size PDF in 1-D percolation, eq. (4), very well, so we change the occupied probability in eq. (4) into a constant *C*, and fit experimental data using the new equation by changing the value of *C*:

$$P(l)=\frac{(1-C)^2}{C}l\mathrm{e}^{\ln C\cdot l} \tag{9}$$

The PDF distribution of fully developed isolated bubbles along wire heaters can be found in fig. 10. As indicated in the figure, obvious differences of bubble footprint size PDF under different heat flux are not observed in all cases, which means the average bubble size can be assumed as a constant for the whole boiling process. The eq. (9) with different value of *C* fits nicely with the experimental data. The average bubble length can be calculated by eq. (5), the calculated average bubble length for each case is 2.33 mm and 3.17 mm, respectively.

The CDF is obtained:

$$C(l)=1+\int P(l)=1+\frac{(1-C)^2}{C\ln C}l\mathrm{e}^{\ln C\cdot l}\left(1-\frac{1}{\ln C}\right) \tag{10}$$

where $C(l)$ can be replaced by a random number $q \in [0, 1]$. Then we can obtain the bubble length l as the input in the MC model by solving eq. (10).

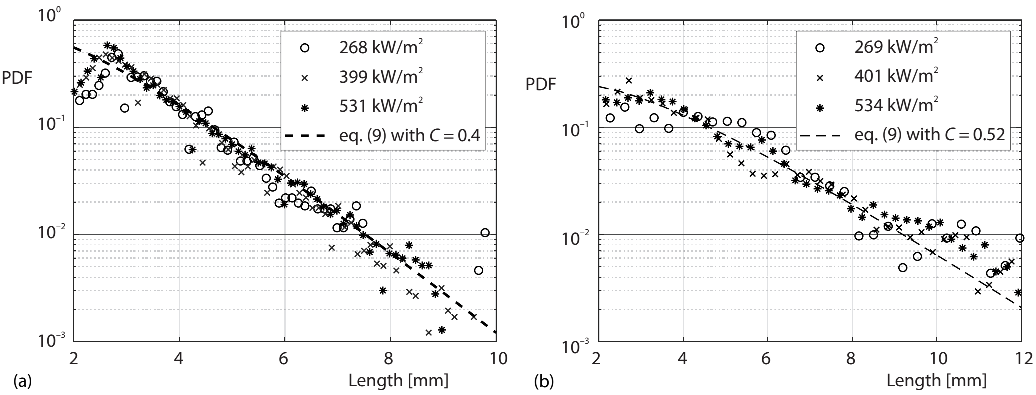

Figure 10. Fully developed isolated bubble size PDF at lower heat flux; (a) free wire heater and (b) sandwiched wire heater

Results and discussions

Bubble footprint size PDF

Both experimental and simulated bubble footprint size PDF under different average heat flux are demonstrated in fig. 11. Experimental results are shown in the left column and simulated results are shown in the right. We pick three different average heat flux stages in each experiment to shown the process from nucleate boiling to boiling crisis (dash line stairs in each subplot). In the simulated results, supercritical case are also indicated (dash-dotted line stairs).

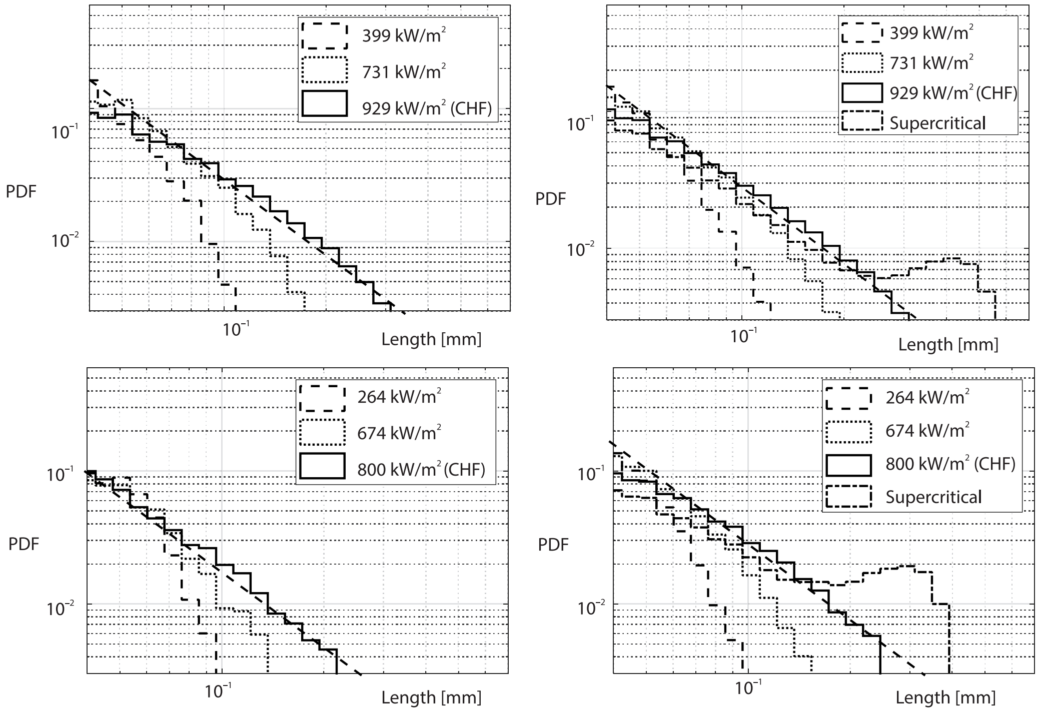

Figure 11. Bubble footprint length PDF distributions at different average heat flux; left and right column shows experimental and simulated results, respectively; free wire heater, sandwiched wire heater cases are separately arranged from top to bottom

We find the power-law distribution at boiling crisis in all cases. The critical exponent is evaluated by the maximum likelihood estimate. For the experimental cases (left column in fig. 11), exponent is found to be 1.87 ±0.01, 1.85 ±0.01, respectively. It is particularly stirring to discover the exponents are around almost a same value in both experimental cases which is a strong evidence that the wire heater pool boiling is a natural continuum percolative process.

In our research, the confined wire heater boiling aims to artificially lead to a stable vapor film earlier than free wire heater by squeezing bubbles, which is actually a manually approach to promote the percolation. Although CHF values are not the same in two cases, we can still observe similar bubble footprint PDF at each boiling crisis. The critical phenomenon seems not to be influenced by different CHF values. This observation inspires us an innovative basic idea in CHF enhancement studies: no matter how high the heat flux is, the CHF would not be reached as long as the percolation transition does not show up.

The predicted PDF distributions in the right column of fig. 11 prove the correctness of the 1-D continuum percolative MC model in simulating experimental PDF. The power-law distributions are also found in simulations, the exponent is estimated as 1.85 ±0.01, 1.79 ±0.01, respectively, which are really close to the experimental values. The supercritical cases are reached by artificially adding nucleation sites into MC simulation, the inputs of $t_g f$ and average bubble size are kept as same values as those in CHF simulations. Risen tails of red stairs represent the vapor film appearances.

Phase transitions in boiling process

Specific to the boiling process, the phase transition refers to phenomena that longest vapor patch growth rate as well as the second longest patch reaches to their maximum values at the percolation transition.

In our research, the phase transition phenomenon is also simulated. Figure 12 shows variations of normalized longest, *L*, and second longest, *SL*, vapor patch along wire heaters under different NSD. Solid lines represent experimental results, and both black and white dots demonstrate simulated trends. The simulated results show good agreement with the experimental results, especially for two bare wire heaters. It is noted that wire heaters become broken in a very short time after the CHF happens (we can always reach a post-CHF stage with a spreading vapor film on bare wire heaters owe to the relative lower CHF, but the wire heater always has a severe deformation due to the burnout, which is impossible for us to obtain the bubble footprint at that time), so solid lines stop at CHF stages, post-CHF stages are continued by adding nucleation sites in to the MC model.

Similar trends are observed in different cases. Specifically, *L* patches keep increasing in the whole process, and their increase rates reach maximum when CHF happen. At the same time, *SL* patches start decreasing after CHF, which is one of hallmarks in continuum percolation criticality [22]. As the NSD become larger, more and more bubbles coalesce with each other, the longest and second longest spanning bubbles compete in absorbing other smaller bubbles, both these two relative lager bubbles keeps growing at this period. At a critical moment, the *L* and *SL* bubbles will finally merge into a larger one, this is when the CHF happens. After the CHF, the new merged *L* bubble will eventually absorb all other small bubbles resulting in a vapor film covering the whole boiling surface (as shown in simulated results in fig. 11, the longest patches cover whole wire heaters at supercritical cases). Thus the maximum of the SL bubble marks the occurrence of the CHF (percolation critical), and it can be considered as one of natural characteristics of the boiling crisis.

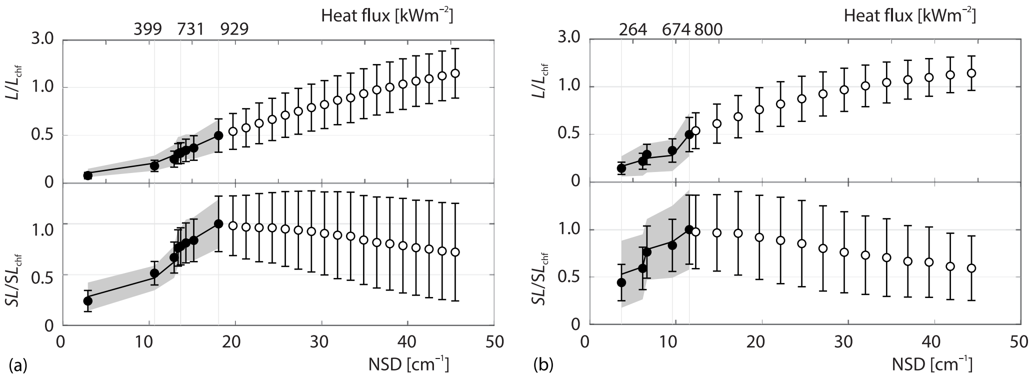

Figure 12. Measured (solid line) and simulated (filled or empty dots) trends of the *L* and *SL* bubbles as a function of the NSD in; (a) free and (b) sandwiched wire

Conclusions

In this research, we promote the percolation phenomenon by placing the wire heater between two parallel glasses. Both wire heater boiling show similar scale-free behaviors (pawer-law distribution with exponent ≈1.86) at boiling crisis. This is the first time we experimentally observe the coincident phenomena at different pool boiling conditions, which shows the boiling crisis is a natural continuum percolative behavior. By post-processing HSV, the number of nucleation sites, $t_g f$ and average bubble length under different average heat fluxes can be obtained as inputs of the 1-D continuum percolative MC model. The MC model successfully simulates the bubble footprint length PDF as well as the phase transition of longest and 2nd longest bubble footprint at percolation critical. Using such a concise model to describe a complex phenomenon can give us a better understanding of the boiling crisis. Current work reveals one of natural characteristics of the boiling crisis, the occurrence of bubble footprint scale-free behavior and the percolation transition could be a criterion predict the CHF. More practically, this research inspires us to improve the CHF limit by suspending the percolative phenomena.

Acknowledgment

The present work is supported by Natural Science Foundation of China (Grant No. 11675127) .The authors thank Prof. Matteo Bucci from MIT NSE department for his enlightening discussions.

Nomenclature

b – random number ∈ [0, 1]
C – parameter in eqs. (9) and (10)/cumulative density function
CHF – critical heat flux, [Wm^2]
f – bubble frequency
L – system scale/longest bubble footprint[m]
l – average length of bubble footprint[m]
n – cluster number density
NSD – nucleation site density, [cm^{-1}]
P – longest cluster density/bubble footprint PDF
P′ – second longest cluster density
p – occupied probability
r – half length of strip in 1-D continuum problem
S – average cluster size
SL – second longest bubble footprint, [m]
s – cluster size
t – time, [s]

Greek letters

ω – probability of a site belongs to a *s*-cluster

Superscript/subscript

g – bubble growth
L – longest cluster
SL – second longest cluster
w – bubble wait

Acronyms

CDF – cumulative density function
HSV – high speed video
PDF – probability density function

References

[1] Collier, J. G., *et al.*, *Convective Boiling and Condensation*, Clarendon Press, Oxford, UK, 1994
[2] Berenson, P. J., Experiments on Pool-Boiling Heat Transfer, *International Journal of Heat and Mass Transfe*r, *5* (1962), 10, pp. 985-999
[3] Liter, S. G., Kaviany M., Pool-Boiling CHF Enhancement by Modulated Porous-Layer Coating: Theory and Experiment, *International Journal of Heat and Mass Transfer*, *44* (2001), 22, pp. 4287-4311
[4] O'Hanley, H., *et al*., Separate Effects of Surface Roughness, Wettability, and Porosity on the Boiling Critical Heat Flux, *Applied Physics Letters*, *103* (2013), 2, pp. 58-67
[5] Lu, M. C., *et a*l. Critical Heat Flux of Pool Boiling on Si Nanowire Array-Coated Surfaces, *International Journal of Heat and Mass Transfer*, *54* (2011), 25-26, pp. 5359-5367
[6] Kutateladze, S. S., On the Transition Film Boiling under Natural-Convection, *Kotloturbostroenie*, *3* (1948), pp. 10-12
[7] Zuber, N., Hydrodynamic Aspects of Boiling Heat Transfer, Ph. D. thesis, University of California, Los Angeles, Cal., USA, 1959
[8] Ahn, H. S., *et al*., Effect of Liquid Spreading Due to Nano/Microstructures on the Critical Heat Flux during Pool Boiling, *Applied Physics Letters*, *98* (2011), 7, pp. 718
[9] Zhang, B. J., Kim, K. J., Effect of Liquid Uptake on Critical Heat Flux Utilizing a 3-D, Interconnected Alumina Nanoporous Surfaces, *Applied Physics Letters*, *101* (2012), 5, pp. 3374

[10] Kim, H. D., Kim, M. H., Effect of Nanoparticle Deposition on Capillary Wicking that Influences the Critical Heat Flux in Nanofluids, *Applied Physics Letters*, *91* (2007), 1, 718
[11] Rahman, M. M., *et al.*, Role of Wickability on the Critical Heat fFlux of Structured Superhydrophilic Surfaces, *Langmuir*, *30* (2014), 37, pp. 11225-11234
[12] Rajvanshi, A. K., *et al*., Investigation of Macrolayer Thickness in Nucleate Pool Boiling at High Heat Flux, *International Journal of Heat and Mass Transfer*, *35* (1992), 2, pp. 343-350
[13] Guan, C. K., *et al.*, A New Mechanistic Model for Pool Boiling CHF on Horizontal Surfaces, *International Journal of Heat and Mass Transfer*, *5*4 (2011), 17-18, pp. 3960-3969
[14] Rahman, M. M., *et al*., Scalable Nanomanufacturing of Virus-Templated Coatings for Enhanced Boiling, *Advanced Materials Interfaces*, *1* (2014), 2, 1300107
[15] Skokov, V. N., *et al.*, Self-Organization of a Critical State and 1/fα-Fluctuations at Film Boiling, *Physics Letters A*, *263* (1999), 4-6, pp. 430-433
[16] Lloveras, P., *et al*., Boiling Crisis as a Critical Phenomenon, *Physical Review Letters*, *108* (2012), 21, 215701
[17] Charignon-, T., *et al*., Criticality in the Slowed-Down Boiling Crisis at Zero Gravity, *Physical Review E*, *91* (2015), 5, 053007
[18] Zhang, L., *et al*., Percolative Scale-Free Behavior in the Boiling Crisis, *Physical Review Letters*, *122* (2019), 13, 134501
[19] Stauffer, D., Aharony A., *Introduction Percolation Theory*, Taylor and Francis, London, UK, 2018
[20] Sahimi, M., *Applications of Percolation Theory*, Taylor and Francis, London, UK, 1994
[21] Bonjour, J., Lallemand, M., Flow Patterns during Boiling in a Narrow Space between Two Vertical Surfaces, *International Journal of Multi-phase Flow*, *24* (1998), 6, pp. 947-960
[22] Kruger, A., Dimensionality in Continuum Percolation Thresholds, Ph. D. thesis, University of Bielefeld, Bielefeld, Germany, 2003

Paper submitted: April 8, 2020
Paper revised: September 25, 2020
Paper accepted: October 3, 2020